

# Systemic change in the Rhine-Meuse basin: Quantifying and explaining parameters trends in the PCR-GLOBWB global hydrological model



Jessica Ruijsch<sup>a,\*</sup>, Judith A. Verstegen<sup>b</sup>, Edwin H. Sutanudjaja<sup>c</sup>, Derek Karssenberg<sup>c</sup>

<sup>a</sup> Water Systems and Global Change Group, Wageningen University & Research, Wageningen, the Netherlands

<sup>b</sup> Laboratory of Geo-Information Science and Remote Sensing, Wageningen University & Research, the Netherlands

<sup>c</sup> Department of Physical Geography, Utrecht University, Utrecht, the Netherlands

## ARTICLE INFO

### Keywords:

Systemic change  
Hydrological modelling  
Parameter stability  
PCR-GLOBWB model  
Rhine-Meuse basin

## ABSTRACT

In hydrological modelling, traditionally one calibration was performed over a certain calibration period before the model is used to study the hydrological system. This implies that a constant model structure and parameterization are assumed. However, if the catchment system is subject to changes that are not incorporated in the model, the parameter values found in a calibration period may not be optimal for other periods, which is called systemic change. The aim of this study was to identify systemic change and its possible causes with the PCR-GLOBWB hydrological model in the Rhine-Meuse basin, by performing a brute-force calibration for multiple periods for five calibration locations between 1901-2010. Systemic change was studied for the main model components, by selecting a key parameter from each component (minimum soil depth fraction, saturated hydraulic conductivity, groundwater recession coefficient, degree day factor, Manning's  $n$ ). These parameters were calibrated for 10-year rolling periods between 1901-2010. The results showed that at the downstream locations, the changes in optimal parameter values were small, while at the upstream locations, the optimal values of most parameters changed considerably over the different rolling calibration periods, signifying systemic change. Especially the degree day factor showed large variations, varying over time between 0.5 and 2.5 times its default value at Basel and Maxau (upstream and middle part of the Rhine basin). Based on correlation analysis, it was found that climate change as well as changes in land use and river structure are possible causes of changes in optimal parameter values through time.

## 1. Introduction

The amount of damage caused by riverine flooding has increased over the past years due to population growth and economic development in flood prone areas (Winsemius et al., 2016). On top of that, anthropogenic climate change and natural climate variability may change atmospheric processes and as a consequence the occurrence of riverine floods (Hall et al., 2014). To be able to adapt to the consequences of climate change, more knowledge is needed on how hydrological systems respond to changing conditions (Blöschl et al., 2019). Hydrological models can help to improve system understanding and to simulate future systems to support decision making. However, due to a lack of data or process understanding, hydrological models need some sort of parameterization to perform well (Arsenault et al., 2018), which is why hydrological models are often calibrated (i.e., finding parameter values that result in the best fit between model output and historic observations of the catchment).

In hydrological modelling, traditionally one calibration with discharge measurements, or possibly additional hydrological information (e.g. Fernandez-Palomino et al., 2020; Ilampooranan et al., 2021; Melišová et al., 2020), is performed over a certain period, after which the model is validated with observations of another period (split-sample test) (Klemeš, 1986; Pechlivanidis et al., 2011). This method implies the modeller assumes that the model equations and parameters are stationary. However, fundamental changes in behaviour of the modelled system, represented by the model equations, can occur over time that are not represented by the used model structure or parameterization. These changes can therefore not be simulated and may result in model output that deviates from observed values. We refer to this problem as 'systemic change', following Verstegen et al. (2016).

The assumption of a stationary system used in split-sample testing becomes invalid under systemic changes and can cause large deviations in hydrological forecasts (Coron et al., 2012; Merz et al., 2011), especially because hydrological models often behave highly nonlinear

\* Corresponding author.

E-mail address: [jessica.ruijsch@wur.nl](mailto:jessica.ruijsch@wur.nl) (J. Ruijsch).

(Peel and Blöschl, 2011). It is therefore increasingly recognized in hydrology that hydrological model equations and parameter values cannot be naively transferred to changing conditions (Thirel et al., 2015).

If an hydrological model is calibrated for different periods and the optimal model parameter values vary over these periods, this can have several causes (Merz et al., 2011; Westra et al., 2014). First, changes in the catchment may have occurred that are not incorporated in the model. Processes like climate change (Peel and Blöschl, 2011), land use change (Pathiraja et al., 2016) and the construction of hydrological structures like dikes (Hall et al., 2014) can affect the hydrological system and, therefore, affect the optimal model parameter values in different calibration periods if these processes are not incorporated in the model. Secondly, if the used representation of catchment processes is too simplistic, the model may not be able to simulate the discharge under changing conditions (Wagener et al., 2003). In addition, model calibration partly compensates for error or bias in input and/or observational data, so if these error terms are not constant through time, performing calibration over different periods may imply different optimal model parameter values (Beven and Binley, 1992; Westra et al., 2014).

Several studies have been carried out to determine the effect of climate change and land use change on optimal model parameter values. Merz et al. (2011) determined the time stability of optimal parameter values for six 5-year periods between 1976 and 2006 in 273 Austrian catchments and found considerable variation in optimal snow and soil moisture parameter values. Sleziak et al. (2018) used three 10-year periods between 1981 and 2010 to determine how hydrological models perform under different climate conditions and found that the optimal model parameter values varied over these periods, especially for the parameters related to snow and soil moisture processes. Pathiraja et al. (2016) studied the effect of deforestation on optimal model parameter values and found that the values of parameters related to groundwater and surface routing changed in response to deforestation, to account for a decrease in percolation and a faster peak discharge.

However, these studies assessed relatively short time spans (e.g., 30 to 40 years) and small study areas (< 6200 km<sup>2</sup>), while non-stationarity may become more apparent when taking longer periods or larger river basins, due to long term or large-scale processes (Peel and Blöschl, 2011). Also, existing studies often explore systemic change in a limited set of hydrologic system components while the focus is often on a small set of possible environmental drivers of systemic change. The latter is an important limitation as systemic change can be due to a range of possible causes, including and not restricted to, climate change, land use change, and basin management. Thus, an analysis studying these changes simultaneously, over large time spans, in large basins as well as smaller subbasins, is needed to determine the possible causes of systemic change, and to prevent incorrect conclusions regarding causal relations.

The aim of this study is, therefore, to identify systemic change and its possible causes for a large river basin and a long period with PCR-GLOBWB 2.0, a global hydrological model (Sutanudjaja et al., 2018; van Beek and Bierkens, 2009; van Beek et al., 2011). The Rhine-Meuse basin (200,000 km<sup>2</sup>) was chosen as study area, because discharge and meteorological observations are available for more than 100 years. This results in the following research questions: (i) provided the PCR-GLOBWB 2.0 model, has systemic change occurred in the Rhine-Meuse basin in the last century? If yes, in what parameters, when and how abrupt; (ii) what is the variation in systemic change (if present) between sub-basins; and (iii) what is the relation of systemic changes (if present) with changes in climate, land use, and river structures?

This study contributes to the existing literature as follows. The long study period (> 100 years) provides the opportunity to detect long-term slow systemic changes in the hydrological system, allowing for a better understanding of how the hydrological system will change to anthropogenic climate change and land use change in the future. This is especially relevant for climate change studies that use global/large-scale hydrological models in a simplified manner. In addition, most existing studies have a relatively small study area and the use of the Rhine-Meuse

basin (200,000 km<sup>2</sup>), through which systemic change can be studied at larger scales. Furthermore, the comparison of trends in optimal parameter values between different sub-basins within the large Rhine-Meuse basin allows for the assessment of spatial variation in systemic change and the relations between these different sub-basins (e.g., upstream vs. downstream).

## 2. Methods

In summary, the PCR-GLOBWB hydrological model (Sutanudjaja et al., 2018; van Beek and Bierkens, 2009; van Beek et al., 2011) (Section 2.2) is run for the Rhine-Meuse basin (Section 2.1) between 1901 and 2010, to perform a brute force calibration of five parameters (Sections 2.3 and 2.4). Measured discharge data are used to calibrate the model at Basel, Maxau, Lobith, Cochem and Borgharen, representing different parts and tributaries of the Rhine-Meuse basin. To be able to identify the temporal stability of the optimal parameter values, the model is calibrated in three different ways:

Default model: no calibration is performed and PCR-GLOBWB is run with its default parameterization;

One calibration: the model is run with 576 different parameter sets to determine the optimal parameter values for 1901-2010;

Rolling calibration: the model is run with 576 different parameter sets to determine the optimal parameter values for each 10-year rolling calibration period (i.e., 1901-1910, 1902-1911, 1903-1912, ..., 2001-2010).

This last calibration method results in a time series of 101 optimal parameter-value sets, which is analysed for trends, as an indication for systemic change. The trends in optimal parameter values at different locations were then compared to patterns in meteorological forcing data, land use data and qualitative data on the construction of river structures, to identify possible causes of the systemic changes (Section 2.5).

### 2.1. Study area: the Rhine-Meuse basin

With a basin area of approximately 185,000 km<sup>2</sup>, the river Rhine is one of the larger rivers in Europe. It originates in the Swiss Alps and flows through several countries (i.a. Switzerland, Germany and the Netherlands) after which it ends in the North Sea. The discharge at the river mouth is on average about 2300 m<sup>3</sup>/s, of which almost 50% comes from the area upstream of Basel (Schmitt et al., 2018). In the most upstream part, the discharge largely depends on glacial and snow melt, while the more downstream sub-catchments have a combined rainfall-snowmelt regime.

The Meuse basin has an area of approximately 35,000 km<sup>2</sup> and is located in France, Belgium, Luxembourg, Germany and the Netherlands (De Niel et al., 2017). The discharge of the Meuse is on average about 350 m<sup>3</sup>/s and the river is mainly fed by rain. This results in high winter discharge and very low summer discharge (about 25% of winter discharge) (De Wit et al., 2007).

The study area contains the combined Rhine-Meuse basin, but excludes the delta area in the Netherlands. In this study area, the Meuse catchment is therefore not a sub-catchment of the Rhine, but a separate catchment. The total Rhine-Meuse basin covers approximately 200,000 km<sup>2</sup> (Fig. 1) The Rhine has always been an important river due to its economic and cultural relevance (Schmitt et al., 2018), but with a notable flood risk that has increased over the past decennia (Murawski et al., 2016). It is expected that the regime will change from a combined rainfall-snowmelt regime to a more rainfall-dominated regime, which is likely to cause an increase in the occurrence of extreme high and low flow (Hurkmans et al., 2009).

### 2.2. Model and input data

The model used in this study was PCR-GLOBWB 2.0, a global hydrological model (Sutanudjaja et al., 2018; van Beek and Bierkens, 2009;

Fig. 1. Map of the combined Rhine and Meuse basin (adapted from: Sutanudjaja et al. (2011)). The orange cities mark the locations used for calibration.



van Beek et al., 2011). This second version of the model is available in a 5-arcminute as well as in a 30-arcminute resolution and simulates the terrestrial water balance on a daily time step. Although a 5-arcminute resolution would arguably result in a closer representation of the real system, a 30-arcminute resolution was chosen for this study to save computation time. For the parameters, the standard input data and parameterisation of PCR-GLOBWB 2.0, as described in Sutanudjaja et al. (2018), was used. This is largely the same as the parameterisation given in van Beek and Bierkens (2009) for PCR-GLOBWB 1.0. The model was run from 1901 to 2010, corresponding to the availability of the discharge measurements used as observational data in the calibration (Section 2.4).

The model consists of 5 modules: the meteorological forcing module, the land surface module, the groundwater module, the surface water routing module, and the irrigation and water use module. In these modules, PCR-GLOBWB calculates with a daily time step the water storage in two soil layers (with a maximum thickness of, respectively, 0.3 and 1.2 m) and the underlying groundwater layer. In addition, the exchange between these layers, snow storage, interception storage and the atmosphere is calculated. The meteorological forcing data set of PCR-GLOBWB 2.0 consists of monthly precipitation, temperature and reference evaporation data from the CRU TS 3.2 data set (Harris et al., 2014) from the Climate Research Unit of the University of East Anglia.

Because the model uses daily time steps, the forcing data was down-scaled to daily values with ERA-20C (Poli et al., 2016). For a more detailed description of the model and its default parameterization, refer to Sutanudjaja et al. (2018).

### 2.3. Calibration parameters

Five model parameters are calibrated: the degree day factor ( $f_d$ ) ( $m^3C^{-1}day^{-1}$ ), saturated hydraulic conductivity ( $k_{s,1}$ ,  $k_{s,2}$ ) ( $mday^{-1}$ ), minimum soil depth fraction ( $f$ ) (-), groundwater recession coefficient ( $J^{-1}$ ) ( $day^{-1}$ ), and Manning's  $n$  ( $n$ ) ( $m^{5/6}s^{-1}$ ) (Table 1). These parameters were selected in such a way that each component of the hydrological system is represented, which allows an evaluation of the occurrence of systemic changes in these different components. For each component, the most important parameter was selected based on Sutanudjaja et al. (2014) and López López et al. (2017). Although including more parameters could result in a better fit between modelled and observed discharge, it would also result in a rapid increase in computation time needed for the brute-force calibration.

PCR-GLOBWB uses a temperature index model to simulate snow melt. This means that the degree day factor ( $f_d$ ) ( $m^3C^{-1}day^{-1}$ ) is used to model snow melt as:

$$SC_{melt} = f_d(T - T_{melt}) \tag{2.1}$$

**Table 1**

Parameters used for calibration and a short description for each parameter.

Parameter	Symbol	Unit	Short description
Degree day factor	$f_d$	$\text{mm}^\circ\text{C}^{-1}\text{day}^{-1}$	Relates the amount of snow melt to the temperature above the freezing point.
Minimum soil depth fraction	$f$	-	Controls the partitioning of liquid rainfall into direct runoff and infiltration to the soil
Saturated hydraulic conductivity	$k_{s,1}, k_{s,2}$	$\text{mday}^{-1}$	Determines the amount of infiltration into the first soil layer and the percolation to the second soil layer and groundwater layer.
Groundwater recession coefficient	$J^{-1}$	$\text{day}^{-1}$	Describes the linear relation between groundwater storage and outflow.
Manning's n	$n$	$\text{m}^{5/6}\text{s}^{-1}$	Roughness coefficient used to simulate the kinematic wave routing.

where  $SC_{melt}$  is the amount of snow melt (m),  $T$  is the actual temperature ( $^\circ\text{C}$ ) and  $T_{melt}$  is the temperature at which snow will melt ( $^\circ\text{C}$ ) (Wada et al., 2014). The degree day factor determines, therefore, the amount of snow melt per degree day. The default value for the degree day factor in PCR-GLOBWB is  $2.5 \text{ mm}^\circ\text{C}^{-1}\text{day}^{-1}$  (Sutanudjaja et al., 2018).

The minimum soil depth fraction  $f$  (-) is used in PCR-GLOBWB to partition the net liquid water reaching the soil – consisting of snowmelt and rainfall – into direct runoff (overland flow above the soil) and infiltration to the soil. Such partitioning processes are conceptualized based on the distribution of soil saturation in each grid cell and following the Improved Arno scheme (Hagemann & Gates, 2003; Todini, 1996). The fraction of saturated soil in a grid cell,  $x$  (-), is given by (Sutanudjaja et al., 2014; van Beek & Bierkens, 2009):

$$x = 1 - \left( \frac{W_{max} - W_{act}}{W_{max} - W_{min}} \right)^{\frac{b}{b+1}} \quad (2.2)$$

where  $W_{max}$  (m) is the total storage capacity of all soil layers,  $W_{min}$  (m) is the minimum storage capacity of the soil layer,  $W_{act}$  (m) is the actual storage of all soil layers, and the exponent parameter  $b$  [-] defines the distribution of soil water storage capacities within a cell. In PCR-GLOBWB,  $W_{max}$  and  $W_{min}$  are related through the minimum soil depth fraction  $f$  (-) as:

$$W_{min} = W_{max} f \quad (2.3)$$

For grid cells with  $f = 0$ , and, therefore,  $W_{min} = 0$ , direct runoff always occurs for a rainfall event. If  $W_{min} > 0$ , no direct runoff occurs as long as  $W_{act}$  does not exceed  $W_{min}$ . The minimum soil depth fraction depends on the land cover type and location and has therefore different values for tall natural vegetation, short natural vegetation, non-paddy irrigated crops and paddy irrigated crops throughout the basin. In the Rhine-Meuse basin, the minimum soil depth fraction has a value ranging between 0.11 and 0.88 for tall natural vegetation, between 0.00 and 0.50 for short natural vegetation, between 0.75 and 0.88 for non-paddy irrigated crops and 0.75 for paddy irrigated crops. The default values of  $f$  for the tall natural vegetation (i.e. forest) land cover are shown in Fig. 2, as an example.

The saturated hydraulic conductivity ( $k_{s,1}, k_{s,2}$ ) ( $\text{mday}^{-1}$ ) of the first and second soil layer were calibrated simultaneously. They are used in PCR-GLOBWB to, respectively, simulate the transport from the first soil layer to the second soil layer and from the second soil layer to the groundwater layer. The amount of infiltration or capillary rise depends on the saturated hydraulic conductivity and the degree of saturation in the soil layers. This means that the saturated hydraulic conductivity determines how much water can infiltrate into the soil and, therefore, the amount of runoff. The values of the standard parameterization of the model were derived from the digital soil map of the world (FAO, 1998) and tabulated data (van Beek and Bierkens, 2009). Over the Rhine-Meuse basin, the saturated hydraulic conductivity varies between  $0.14$  and  $3.14 \text{ mday}^{-1}$  at the first soil layer and  $0.10$  and  $2.36 \text{ mday}^{-1}$  at the second soil layer (Fig. 2).

The groundwater recession coefficient ( $J^{-1}$ ) ( $\text{day}^{-1}$ ) is used in the groundwater module to quantify the linear relation between groundwater storage and outflow (Sutanudjaja et al., 2018). The default

value of the groundwater recession coefficient depends on aquifer and flow network properties and is computed with the drainage theory of Krajenhoff van de Leur (1958) and lithological maps (Dürr et al., 2005). The default value of the groundwater recession coefficient varies between  $0.003$  and  $0.054 \text{ day}^{-1}$  (Fig. 2).

Manning's  $n$  ( $n$ ) ( $\text{m}^{5/6}\text{s}^{-1}$ ) is a roughness coefficient to simulate the kinematic wave routing in PCR-GLOBWB. The kinematic wave is an approximation of the Saint-Venant equations, where the flow is described by the Manning's equation. The default value of Manning's  $n$  is set to  $0.04 \text{ m}^{5/6}\text{s}^{-1}$  for the entire area, which is a commonly assumed value for natural rivers (Chow, 1959).

#### 2.4. Calibration and sensitivity analysis

The model was calibrated using a brute-force calibration technique, meaning that the model was run for all possible parameter combinations, given a certain step-size (Table 2), for the 1901-2010 period. Since the minimum soil depth fraction, the saturated hydraulic conductivity and the groundwater recession coefficient are spatially variable, the calibration is performed by multiplying the parameter value in each cell with a multiplication factor to retain the spatial pattern of the parameters. The step-size for the multiplication factors follows a linear (constant step-size) scale with multiplication factors of 0.5, 1.0, 2.0 and 3.0, except for the saturated hydraulic conductivity and groundwater recession coefficient, which follow a logarithmic scale because these parameters vary naturally over multiple orders of magnitude (Table 2). This means that these parameters vary with  $10^A$ , where  $A$  is the multiplication factor given in Table 2. The multiplication factors for these parameters is -0.5, 0.0 and 0.5. Combining all these parameter sets results in a total of 576 parameter value combinations that are used for calibration.

To gain more insight into the effect of variation in the parameter values on the hydrograph, a sensitivity analysis was carried out for each of the selected parameters (minimum soil depth fraction, saturated hydraulic conductivity, groundwater recession coefficient, degree day factor and Manning's roughness coefficient). Hereto, we applied a one-at-a-time sensitivity analysis, by running the model for different values for each parameter (Table 2), while the other parameters are set to their default values. For these parameter combinations, the mean yearly average, the mean yearly standard deviation and the mean yearly 95- and 5-percentile of the discharge were calculated. In addition, the resulting hydrographs were plotted for a single year (1930) to show how sensitive the discharge is to the changing parameters, which is important information when interpreting the parameter trends through time. The sensitivity analysis was performed for Basel, representing the upstream areas of the basin, and Lobith, representing the downstream areas, to compare the effect of the parameters on the discharge at different sub-catchments of the study area.

To determine the optimal parameter value combinations of the brute-force calibration, simulated discharge values were compared to observed discharge values from the Global Runoff Data Centre (GRDC; <http://www.bafg.de/GRDC>) at Basel (Rhine), Maxau (Rhine), Lobith (Rhine), Cochem (Moselle) and Borgharen (Meuse). The objective function used to determine the 'optimal' parameter values was the Kling Gupta Efficiency (KGE) (Gupta et al., 2009), which is a decomposition

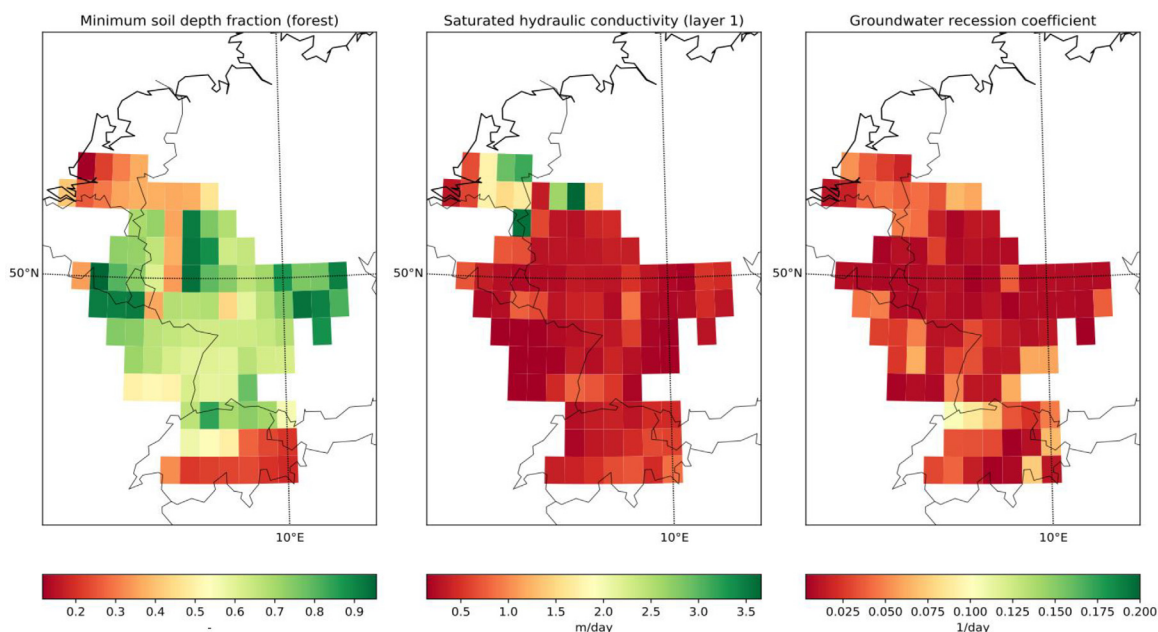


Fig. 2. Spatial distribution of the default values used in PCR-GLOBWB for three calibrated parameters: minimum soil depth fraction for forest (left), saturated hydraulic conductivity of the first layer (centre) and the groundwater recession coefficient (right).

Table 2

Overview of multiplication factors and parameter values used for brute force calibration. For the spatial parameters (minimum soil depth fraction, saturated hydraulic conductivity and groundwater recession coefficient), the shown parameter value is an average over the whole study area and different layers.

	Unit	Scale	Parameter value (multiplication factor)			
			#1	#2	#3	#4
Minimum soil depth fraction	-	Linear	$5.2 \cdot 10^{-1}$ (0.5)	$1.0 \cdot 10^0$ (1)	$2.1 \cdot 10^0$ (2)	$3.1 \cdot 10^0$ (3)
Saturated hydraulic conductivity	$\text{mday}^{-1}$	Logarithmic	$1.6 \cdot 10^{-1}$ (-0.5)	$5.1 \cdot 10^{-1}$ (0)	$1.6 \cdot 10^0$ (0.5)	- (-)
Groundwater recession coefficient	$\text{day}^{-1}$	Logarithmic	$7.8 \cdot 10^{-3}$ (-0.5)	$2.5 \cdot 10^{-2}$ (0)	$7.8 \cdot 10^{-2}$ (0.5)	- (-)
Degree day factor	$\text{mC}^{-1}\text{day}^{-1}$	Linear	$1.3 \cdot 10^{-3}$ (0.5)	$2.5 \cdot 10^{-3}$ (1)	$5.0 \cdot 10^{-3}$ (2)	$7.5 \cdot 10^{-3}$ (3)
Manning's n	$\text{m}^{5/6}\text{s}^{-1}$	Linear	$2.0 \cdot 10^{-2}$ (0.5)	$4.0 \cdot 10^{-2}$ (1)	$8.0 \cdot 10^{-2}$ (2)	$1.2 \cdot 10^{-1}$ (3)

of the Nash-Sutcliffe Efficiency (NSE) and measures correlation, variability and bias to determine the overall model's skill. The KGE was chosen instead of the often used NSE, because the NSE tends to underestimate runoff peaks due to an underestimation of the discharge variability (Gupta et al., 2009).

In this study, three calibration scenarios were compared. The first scenario is no calibration at all, which means the discharge is modelled with the default parameterization of PCR-GLOBWB, which we called the 'default model'. Next, the model was calibrated once for the entire 1901-2010 period, by choosing the parameter value combination with the highest KGE for this whole period, referred to as 'one calibration'. In addition, to determine how the optimal parameter values vary over time, the model was calibrated for consecutive 10-year rolling periods. 10-year periods were used instead of one-year periods, because some processes, like groundwater, respond over larger time scales. By considering at 10-year periods, the calibration period is larger than the residence time of the groundwater. This means that the optimal parameter combination was determined with the objective function evaluated for 1901-1910, 1902-1911, 1903-1912, ..., or 2000-2010 (Lavenne et al., 2016), which we call the 'rolling calibration'. This resulted in 101 optimal parameter value sets, one for each period, represented by its central year.

### 2.5. Identifying systemic change and its causes

Next, the optimal parameter values of the one calibration and rolling calibration were compared to the default model. 'Optimal' parameter

values are the parameter values forming the ensemble of the 10% highest KGE values for each calibration period. This ensemble was used instead of the single optimal parameter value, because one optimal parameter is still for a large part subject to randomness, especially when the KGE values are close together. The mean and standard deviation of the parameter values in this ensemble were plotted for each 10-year rolling calibration period, after which they were visually inspected to detect parameter trends through time. Potential variations in optimal parameter values through time are an indication of systemic change. This method was repeated for all five calibration locations (Basel, Maxau, Lobith, Cochem and Borgharen) and the parameter trends were compared for these locations to determine the spatial variation of systemic change in the Rhine-Meuse basin. However, because the saturated hydraulic conductivity, minimum soil depth fraction and groundwater recession coefficient are spatially variable, the multiplication factors were used for further calculations in the next steps instead of the actual optimal parameter values.

Even though the parameters of the default model and one calibration scenarios do not change through time, their KGE values were calculated for each 10-year rolling calibration period. This enables a comparison of the performances of the default model, one calibration and the rolling calibration scenarios for each 10-year rolling calibration period.

To evaluate the model performance, flow duration curves (i.e. plot of exceedance probability vs. discharge) were plotted for the different calibration scenarios. Following Yilmaz et al. (2008) and Pfannerstill et al. (2014), the mean discharge of the 5- and 95-percentile segments and their bias with the measured discharge was computed for

these calibration scenarios. In addition, hydrographs were plotted for the observed discharge, the default model, one calibration, and rolling calibration, in order to compare the model performance on different aspects of the hydrograph. For the rolling calibration, a discharge series is created by combining the years in the middle of the rolling calibration periods (e.g. 1905 from 1901-1910 and 1906 from 1902-1911), because the middle years represent the surrounding rolling calibration period best. To reduce the number of figures, plots are shown only for Basel and Lobith, respectively representing the upstream and the combined downstream and upstream part of the basin. Figures for the other locations are presented in the digital supplement.

To determine potential causes of systemic change, the optimal parameter value trends are compared to trends in meteorological forcing data from the CRU TS 3.2 data set (Harris et al., 2014) and land use change from the HYDE 3.2 data set (Klein Goldewijk et al., 2011). In addition to the standard meteorological forcing data from PCR-GLOBWB (temperature, precipitation and reference potential evapotranspiration), also the amount of snowfall, defined as the amount of precipitation that falls when the temperature is below 0 °C, and the 90-percentile precipitation were calculated to give more insight into the changing precipitation patterns (Isotta et al., 2014). These values were averaged over the upstream area of each calibration location and over each calibration period to be able to match them to the optimal parameter values.

Furthermore, the optimal parameter value trends are compared to trends in land use areas from HYDE. The HYDE 3.2 database contains the area of cropland, grazing and urban area and an uncertainty range for each 5-arcminute grid cell at 10-year intervals between 1900 and 2010 (i.e. 1900, 1910, 1920 etc.). To be able to compare the land use types for the different calibration locations, the total area of vegetation cover per grid cell was converted to a fraction, by dividing the value by the total cell area. In addition, the dataset was upscaled to a 30-arcminute resolution for the Rhine-Meuse basin with a nearest neighbour interpolation. As with the meteorological data, the upstream average value was calculated for each calibration location.

The trends in climate variables and land use were compared to the trends in optimal parameter values by creating scatter plots for the different calibration locations. The correlation coefficient ( $r$ ) was calculated for each parameter-climate variable/land use type combination to indicate the correlation between these factors. Again, only the figures for Basel and Lobith are shown. The other locations are included in the digital supplement.

### 3. Results

#### 3.1. Sensitivity analysis

Changing parameter values affect the hydrograph in different ways at different locations (Fig. 3; Digital supplement I). The minimum soil depth fraction, groundwater recession coefficient and Manning's  $n$  all have a similarly small effect on the hydrograph at Basel, but at Lobith, the differences in discharge between the parameter multiplication factors are larger. A decrease in the multiplication factor of Manning's  $n$  causes, for example, a delay in the modelled peak discharge at Lobith. The saturated hydraulic conductivity and degree day factor have a large effect on the hydrograph compared to the other parameters. As can be expected, a decrease in saturated hydraulic conductivity results in a peakier discharge at both Basel and Lobith. The effect of changing the degree day factor is most visible during spring and early summer, as a decrease in degree day factor causes a later peak discharge in spring.

The one-at-a-time sensitivity analysis shows that the saturated hydraulic conductivity has a relatively large effect on the mean and extreme discharge values at all locations compared to the other parameters (Digital supplement II). In addition, the minimum soil depth fraction has a larger effect on the mean than on the extreme discharges. The degree day factor is more sensitive at the upstream locations (Basel, Maxau) than at the downstream locations (Cochem, Borgharen) (Fig. 3). Sensi-

tivity analysis of the calibration parameters on the hydrograph for the year 1930 at Basel (left) and Lobith (right). The different rows show different parameters, where the multiplication factors (colours) of that parameter change, while the other parameters remain constant. For the sensitivity analysis at the other locations, refer to Digital supplement I.

#### 3.2. Variations in optimal parameter values

For the default parameterization of PCR-GLOBWB, the KGE value over the 1901-2010 period is 0.374 at Cochem and 0.628 at Maxau. Calibrating the model for this same period results in an increase in KGE at all calibration locations (Table 3). This increase in KGE is largest at Cochem, from 0.37 to 0.57, and smallest at Maxau, from 0.63 to 0.69.

Although the one-calibration outperforms the default scenario continuously, the difference in KGE values between them varies considerably through time, e.g. between 0.64 and 0.35 at Basel for the default model (Fig. 4, A1-A5). The rolling calibration results in a higher or similar KGE value compared to the one calibration scenario, with the highest maximum increase of 0.13 in Basel. At Borgharen, the KGE value hardly increases with the rolling calibration scenario compared to one calibration, with a maximum increase of 0.01. Furthermore, the increase in KGE value is not constant through time. At Basel, for example, the KGE difference between one calibration and rolling calibration is lower at the beginning of the 20<sup>th</sup> century than at the end. For the rolling calibration, the mean values of the 10% optimal parameter multiplication factors vary over time for all parameters (Fig. 4, B1-F5). Generally, this variation is larger at the upstream calibration locations (Basel and Maxau) than at the downstream locations (Lobith, Cochem and Borgharen).

The calibration results are presented as multiplication factors as well as the corresponding actual parameter values (between brackets), averaged over the modelling domain. For the saturated hydraulic conductivity and minimum soil depth fraction the value is also averaged over the different layers explained in Section 2.3. The mean optimal multiplication factor of the minimum soil depth fraction decreases slightly over time at Basel (from 3.0 (2.95 [-]) to 2.5 (2.46 [-])) and Maxau (from 2.9 (2.89) to 2.3 (2.29)). Similarly, the mean optimal multiplication factor of saturated hydraulic conductivity decreases from 0.22 (0.62 mday<sup>-1</sup>) to 0.07 (0.44 mday<sup>-1</sup>) at Basel and 0.23 (0.68 mday<sup>-1</sup>) to 0.01 (0.41 mday<sup>-1</sup>) at Maxau. Also, the mean optimal multiplication factor of the groundwater recession coefficient decreases over time at Basel, but with more variation compared to the minimum soil depth fraction and the saturated hydraulic conductivity. In contrast, at Maxau, the mean optimal multiplication factor of the groundwater recession coefficient is varying between 0.23 (0.06 day<sup>-1</sup>) and -0.27 (0.02 day<sup>-1</sup>) without clear increasing or decreasing trends. The mean optimal multiplication factor of the degree day factor exhibits the highest variation of all parameters at the upstream locations. Both at Basel and Maxau, the mean optimal multiplication factor of the degree day factor starts to increase around 1920 and reaches its peak around 1970, after which it decreases again. The mean multiplication factor of the degree day factor varies between about 0.6 (1.50 mm°C<sup>-1</sup>day<sup>-1</sup>) and 2.6 (6.50 mm°C<sup>-1</sup>day<sup>-1</sup>) at Basel and 0.7 (1.75 mm°C<sup>-1</sup>day<sup>-1</sup>) and 2.6 (6.50 mm°C<sup>-1</sup>day<sup>-1</sup>) at Maxau throughout the calibration period. The mean optimal multiplication factor of Manning's  $n$  shows a constant value of approximately 1.7 (0.07 m<sup>5/6</sup>s<sup>-1</sup>) over the whole period at Basel and a steadily decreasing pattern at Maxau.

At the downstream calibration locations (Lobith, Cochem and Borgharen), the parameters vary less through time compared to the upstream locations. Especially at Borgharen, the mean optimal multiplication factors are steady and close to the values of one calibration. At Lobith, some small variations can be observed, especially for Manning's  $n$ , but no clear patterns over time can be seen. The parameter values at Cochem are relatively constant, except for a sharp decrease in the mean optimal multiplication factor of the saturated hydraulic conductivity and groundwater recession coefficient and an increase in the mean optimal multiplication factor of Manning's  $n$  around 1990.

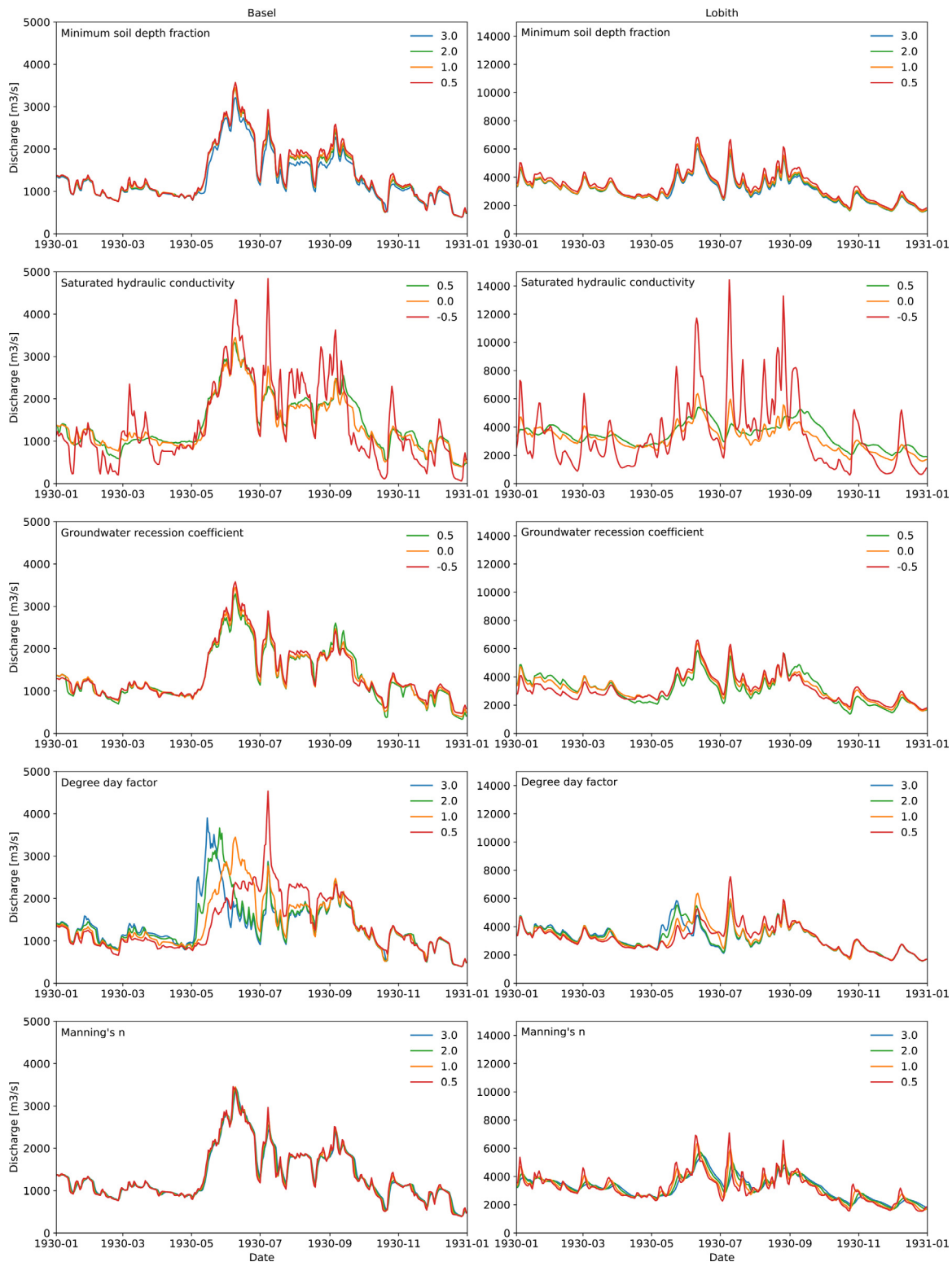


**Fig. 3.** Sensitivity analysis of the calibration parameters on the hydrograph for the year 1930 at Basel (left) and Lobith (right). The different rows show different parameters, where the multiplication factors (colours) of that parameter change, while the other parameters remain constant. For the sensitivity analysis at the other locations, refer to Digital supplement I.

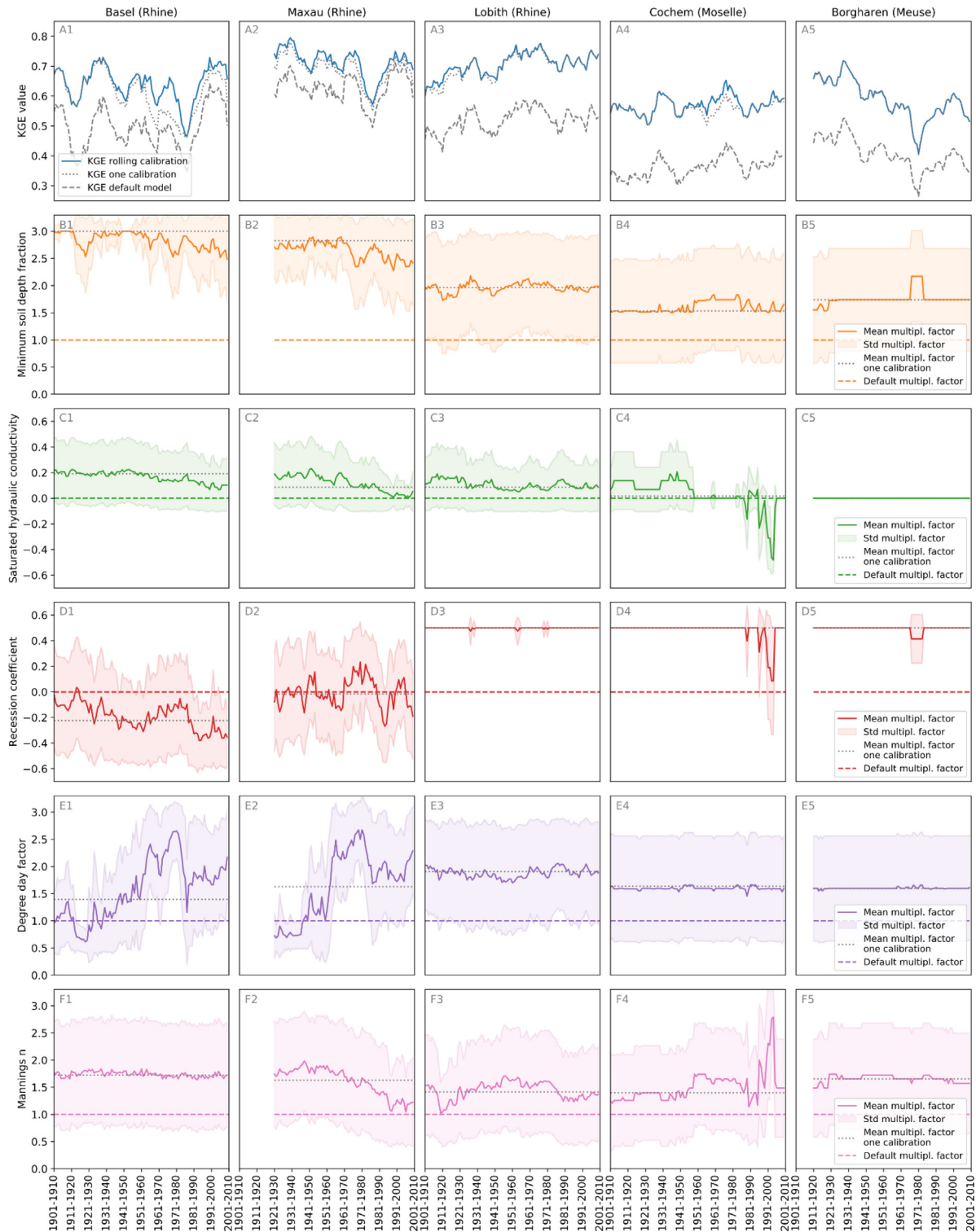


**Fig. 4.** Calibration results at Basel, Maxau, Lobith, Cochem and Borgharen. The KGE values of the default model, one calibration and rolling calibration for each 10-year rolling calibration period are shown in the top row (A1-A5). The mean and standard deviation of the 10% optimal parameter multiplication factors for one calibration, and the default multiplication factor are shown in the other rows. The different parameters are: minimum soil depth fraction (B1-B5), saturated hydraulic conductivity (C1-C5), groundwater recession coefficient (D1-D5), degree day factor (E1-E5) and Manning's n (F1-F5).

**Table 3**

Calibration results for the one calibration scenario between 1901 and 2010. The table shows the KGE of the default model, the KGE value if one calibration is performed over the 1901-2010 period and the mean multiplication factors of the 10% optimal model runs of the different calibration parameters. Because of the spatial variability of the minimum soil depth fraction, the saturated hydraulic conductivity and the groundwater recession coefficient, the multiplication factors are reported instead of the actual parameter values. The value between brackets is the calculated mean upstream optimal parameter value corresponding to these multiplication factors.

Location	KGE default model	KGE one calibration	KGE increase	Mean multiplication factors – One calibration scenario (mean upstream optimal parameter values)				
				Minimum soil depth fraction	Saturated hydraulic conductivity	Groundwater recession coefficient	Degree day factor	Manning's n
Basel	0.50	0.61	0.11	3.00 (2.9)	0.19 (0.58 m day <sup>-1</sup> )	-0.22 (0.023 day <sup>-1</sup> )	1.40 (3.5 mm°C <sup>-1</sup> day <sup>-1</sup> )	1.72 (0.089 m <sup>5/6</sup> s <sup>-1</sup> )
Maxau	0.63	0.69	0.07	2.86 (2.8)	0.09 (0.49 m day <sup>-1</sup> )	-0.02 (0.033 day <sup>-1</sup> )	1.63 (4.1 mm°C <sup>-1</sup> day <sup>-1</sup> )	1.63 (0.065 m <sup>5/6</sup> s <sup>-1</sup> )
Lobith	0.53	0.70	0.18	1.97 (2.0)	0.09 (0.50 m day <sup>-1</sup> )	0.50 (0.078 day <sup>-1</sup> )	1.91 (4.8 mm°C <sup>-1</sup> day <sup>-1</sup> )	1.41 (0.046 m <sup>5/6</sup> s <sup>-1</sup> )
Cochem	0.37	0.57	0.19	1.53 (1.6)	0.02 (0.30 m day <sup>-1</sup> )	0.50 (0.058 day <sup>-1</sup> )	1.64 (4.1 mm°C <sup>-1</sup> day <sup>-1</sup> )	1.40 (0.056 m <sup>5/6</sup> s <sup>-1</sup> )
Borgharen	0.43	0.61	0.19	1.74 (1.9)	0.00 (0.32 m day <sup>-1</sup> )	0.50 (0.057 day <sup>-1</sup> )	1.59 (4.0 mm°C <sup>-1</sup> day <sup>-1</sup> )	1.66 (0.066 m <sup>5/6</sup> s <sup>-1</sup> )

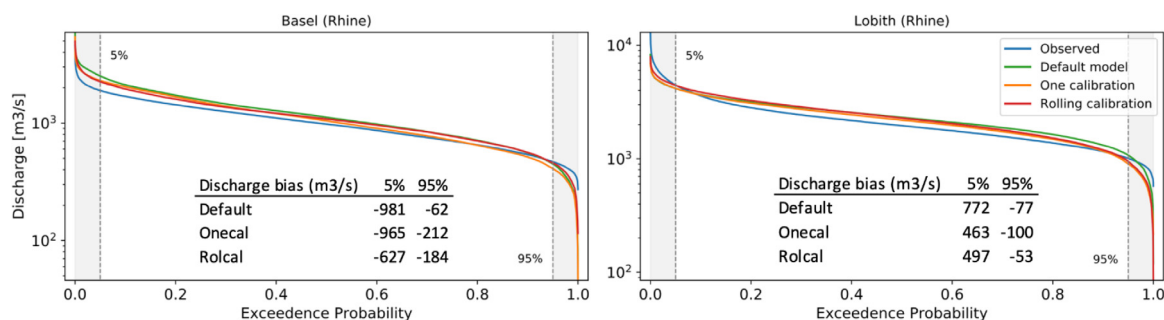


**Fig. 5.** Flow Duration Curve for the different calibration methods (observed, default model, one calibration, and rolling calibration) over the 1901-2010 calibration period at Basel (top) and Lobith (bottom). For the flow duration curve at the other locations, refer to Digital supplement III. The discharge bias of the 0-5% and 95-100% segments (e.g. mean discharge of the default model – mean discharge of the observations) is included in the graphs.

### 3.3. Effect on hydrograph

Both at Basel and at Lobith, the flow duration curve resulting from the model calibrated with a rolling calibration is generally closest to the curve resulting from the observed discharged (Fig. 5; Digital supplement III), also for the high- and low-flow segments, although this is not the case for the low flow (95%) segments at Basel where the bias between the default model and the observed discharge is lower than for the rolling calibration and the high flow (5%) segment at Lobith. There, the bias of the one calibration scenario is slightly less than for the rolling calibration.

At a daily timescale (Fig. 6; Digital supplement IV), the hydrographs predicted with the model based on one calibration and a rolling calibration are very similar for Basel in 1930-1931, but further apart in 1980-1981, especially in the spring of 1980. For this period, the discharge peaks computed with the model based on a rolling calibration occur earlier and are higher than the peaks computed with the model based on one calibration. At Lobith, the hydrograph predicted with the model based on a rolling calibration is less smooth than hydrograph predicted with the model based on one calibration for both 1930-1931 and 1980-1981.

### 3.4. Relations of optimal parameter values with catchment changes

The temperature as well as the amount of precipitation has increased over time at both Basel and Lobith in the past decade (Fig. 7; Digital supplement V). The relative increase in temperature between 1901 and 2010 is largest at Basel, from 6.01 °C in 1901-1910 to 7.97 °C in 2001-2010. The amount of precipitation increased by 3.6% between the 1901-1910 and 2001-2010 at Basel. The reference potential evapotranspiration increased until it peaked around 1940, then decreased rapidly and started rising again around 1980, caused by an incomplete and limited coverage of observational data in the early 20<sup>th</sup> century (Harris et al.,

2014). At both Basel and Lobith, the upstream average amount of snowfall decreased over time in the past decade.

The relative abundance of different land use types has changed largely between 1900 and 2010 (Fig. 8; Digital supplement VI). The fraction of urban area, for example, increases from 0.006 in 1900 to 0.018 in 2010 at the upstream area of Basel and from 0.010 to 0.029 at Lobith. At the same time, the fractions of cropland, grazing area decrease. Especially upstream of Lobith, a rapid decrease in grazing and pasture area can be observed between 1940 and 1960. The total area of landcover changed by human influences (i.e. the sum of urban area, grazing, pasture and cropland) shows a decrease to about 50% of its original value between 1900 and 2010.

The correlations of the mean optimal multiplication values of the parameter found in the rolling calibration with the precipitation (Fig. 9; Digital supplement VII) are generally low, ranging from -0.23 to 0.17 at Basel and Lobith. At Basel, the temperature shows a higher correlation with the saturated hydraulic conductivity (-0.45) and groundwater recession coefficient (-0.49), but these correlations are low at Lobith. The highest correlations can be found between 90-percentile precipitation and the saturated hydraulic conductivity at Basel (-0.75). But also the other parameters are highly correlated with the potential reference evapotranspiration, compared to the other climate variables. At Lobith, the correlations are, except for the degree day factor, lower in comparison to the correlations at Basel.

The correlations between the fractions of upstream land use and the mean optimal multiplication factor of the parameters are generally higher than for the climate variables, especially for Basel, with an *r* value ranging up to -0.87 and 0.89 (Fig. 10; Digital supplement VIII). The highest correlations occur for the saturated hydraulic conductivity with the fraction of urban area, cropland, grazing area and area of total landcover changed by human influences and between the degree day factor and cropland or area of total landcover changed by human influences.

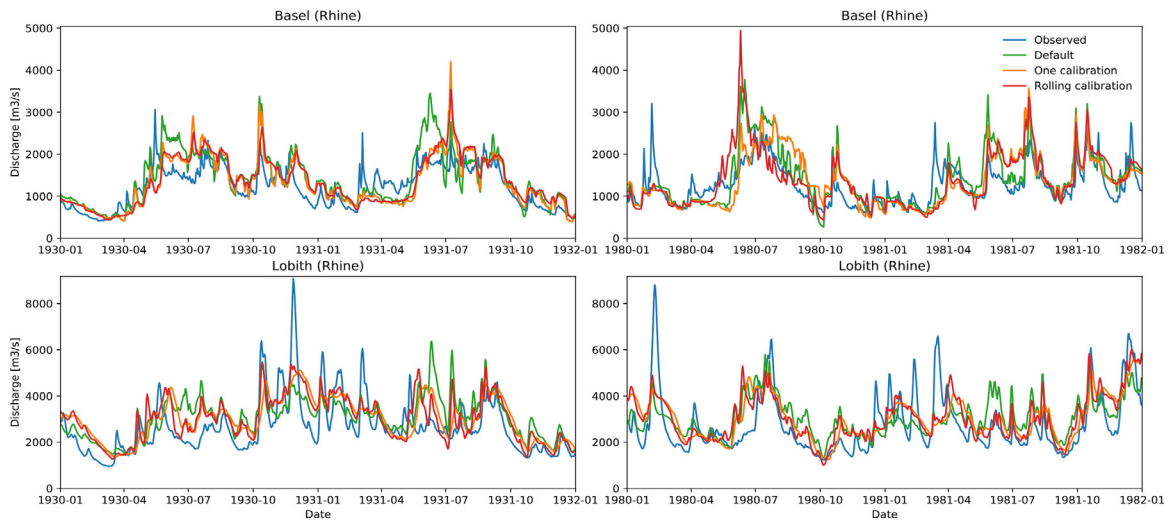


Fig. 6. Hydrographs for the observed discharge, default model, one calibration and rolling calibration for 1930-1931 (left) and 1980-1981 (right) at Basel (top) and Lobith (bottom). For the hydrographs at the other locations, refer to Digital supplement IV.

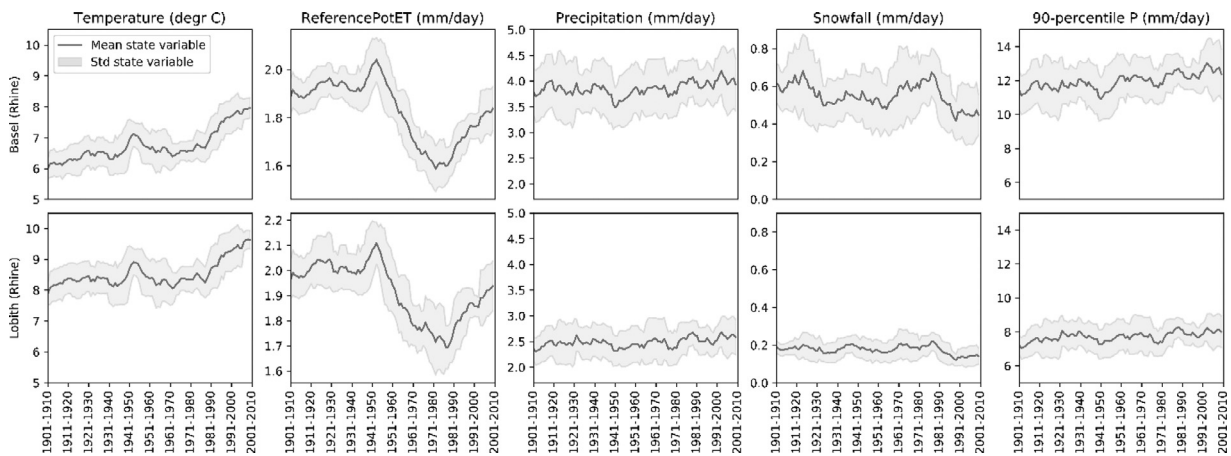


Fig. 7. Mean and standard deviation of climate variables averaged over the 10-year rolling calibration period for the area upstream of Basel (top) and Lobith (bottom). For the climate variables at the other locations, refer to Digital supplement V.

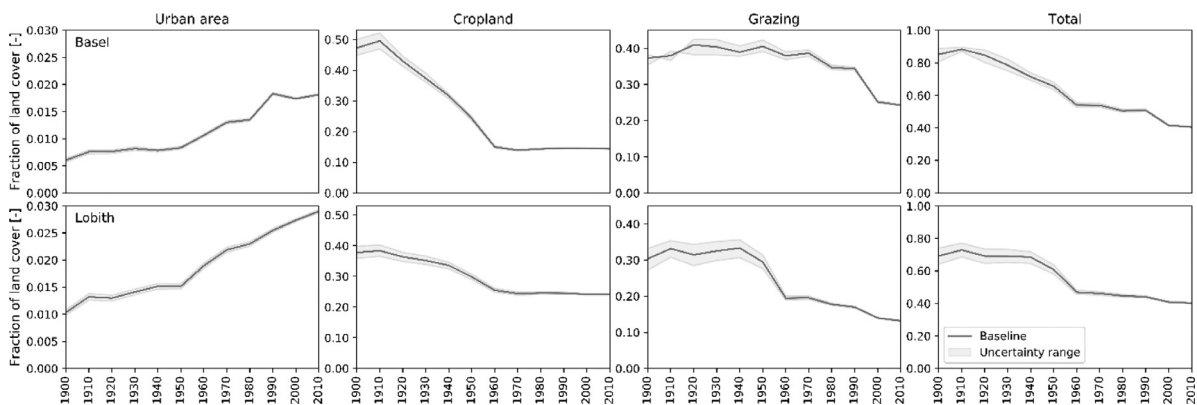


Fig. 8. Fraction of different land use types and its uncertainty range based on literature (Klein Goldewijk et al., 2011) in the upstream areas of Basel (top) and Lobith (bottom). The rightmost column shows the sum of the urban area, cropland, grazing area and pasture, so it represents the total area of landcover changed by human influences. For the patterns in land use at the other locations, refer to Digital supplement VI.

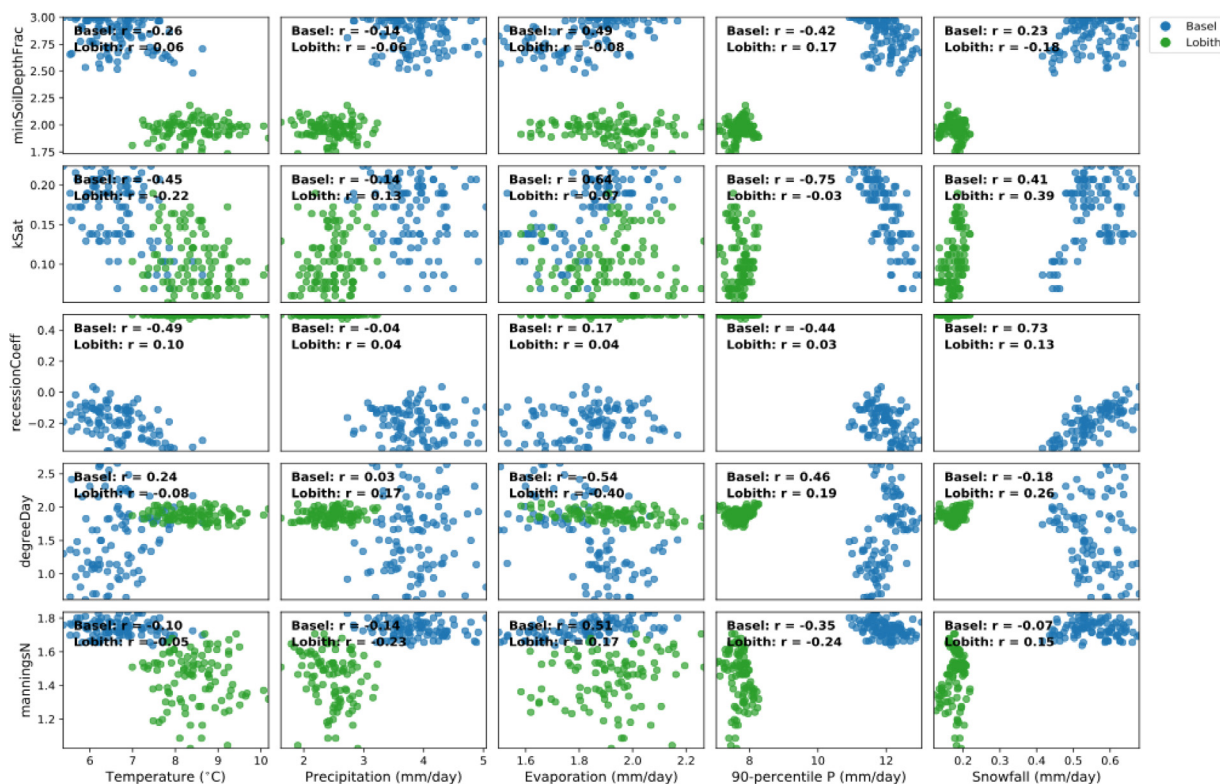


Fig. 9. Scatter plot of parameter multiplication factors and different climate variables for Basel (blue) and Lobith (green) and the corresponding correlation coefficient ( $r$ ). Each dot represents one of the 10-year rolling calibration periods. For the scatter plots at the other locations, refer to Digital supplement VII. (For interpretation of the references to color in this figure legend, the reader is referred to the web version of this article.)

## 4. Discussion

### 4.1. Systemic change and its spatial patterns

Running PCR-GLOBWB with its default parameterization for the Rhine-Meuse basin between 1901 and 2010 causes the model performance to be highly variable through time. Calibrating the model once for the 1901-2010 period increases its overall performance, but the temporal variations in KGE remain, to a large extent, similar. If the model is calibrated for 10-year rolling periods, the KGE values increase for some periods at the upstream locations (Basel, Maxau), the fluctuating model performance cannot be solved by it entirely.

The largest fluctuations in optimal parameter values at the upstream locations were found for the degree day factor, to which the discharge is also most sensitive. At the downstream locations (Lobith, Cochem and Borgharen), the parameters are less variable through time, resulting in a smaller increase in KGE value if a rolling calibration is used. The time variant model parameters indicate that the discharge cannot be accurately predicted with a constant model parameterization throughout the 1901-2010 period, which is, according to the definition of Verstege et al. (2016), an indication for the occurrence of systemic change at the upstream parts of the basin.

The found changes in the optimal value of the degree day factor match the findings of Merz et al. (2011), who calibrated 273 catchments in Austria between 1976 and 2006. Although the magnitude of the change in Merz et al. (2011) is different, with a degree day factor ranging between 1.6 and 1.8 mm°C<sup>-1</sup>day<sup>-1</sup> for Merz et al. (2011) and between 1.5 and 6.5 mm°C<sup>-1</sup>day<sup>-1</sup> for this study, the general pattern is similar to the trends found in this study, indicating similar trends for the Swiss and Austrian Alps. This can possibly be explained by the fact that snow melt in PCR-GLOBWB is largely based on the snow melt module of the HBV model (Bergström, 1995; Wada et al., 2014), which is also used by Merz et al. (2011). Merz et al. (2011) also

found, however, an increase in maximum soil moisture storage, which does not agree with the decrease in minimum soil depth fraction and saturated hydraulic conductivity found at the upstream areas in this study.

### 4.2. Possible causes of systemic change

#### 4.2.1. Climate change

The highest correlations, with  $r$  values higher than 0.5 or lower than -0.5, could be found between the reference potential evapotranspiration and the saturated hydraulic conductivity, degree day factor and Manning's  $n$ , between the 90-percentile precipitation and the saturated hydraulic conductivity and between the amount of snowfall and the groundwater recession coefficient. These correlations indicate that climate change is a potential cause of changing optimal parameter values. However, because precipitation, temperature and reference evapotranspiration are directly used as input variables of PCR-GLOBWB, the model should be able to account for changes in processes like snowmelt and infiltration due to climate change. This implies that the climate change is an indirect cause of the changes in optimal parameter values.

For example, the decrease in saturated hydraulic conductivity and, to a lesser extent, the minimum soil depth fraction, could be explained by an increase in precipitation intensity, as indicated by the high negative correlation with the 90-percentile precipitation. Several studies found an increase in high intensity precipitation events throughout the 20<sup>th</sup> century as a result of temperature increases, both for Europe in general (Klein Tank and Können, 2003) and for the Swiss alps (Scherrer et al., 2016; Schmidli and Frei, 2005). This can partly be observed by an increase in 90-percentile precipitation, but because PCR-GLOBWB uses daily time steps, changes in high intensity precipitation on, for example, an hourly scale, are not taken into account. The resulting increase in infiltration excess overland flow can, therefore, not be accurately simulated, which is compensated by a decrease in the optimal parameter

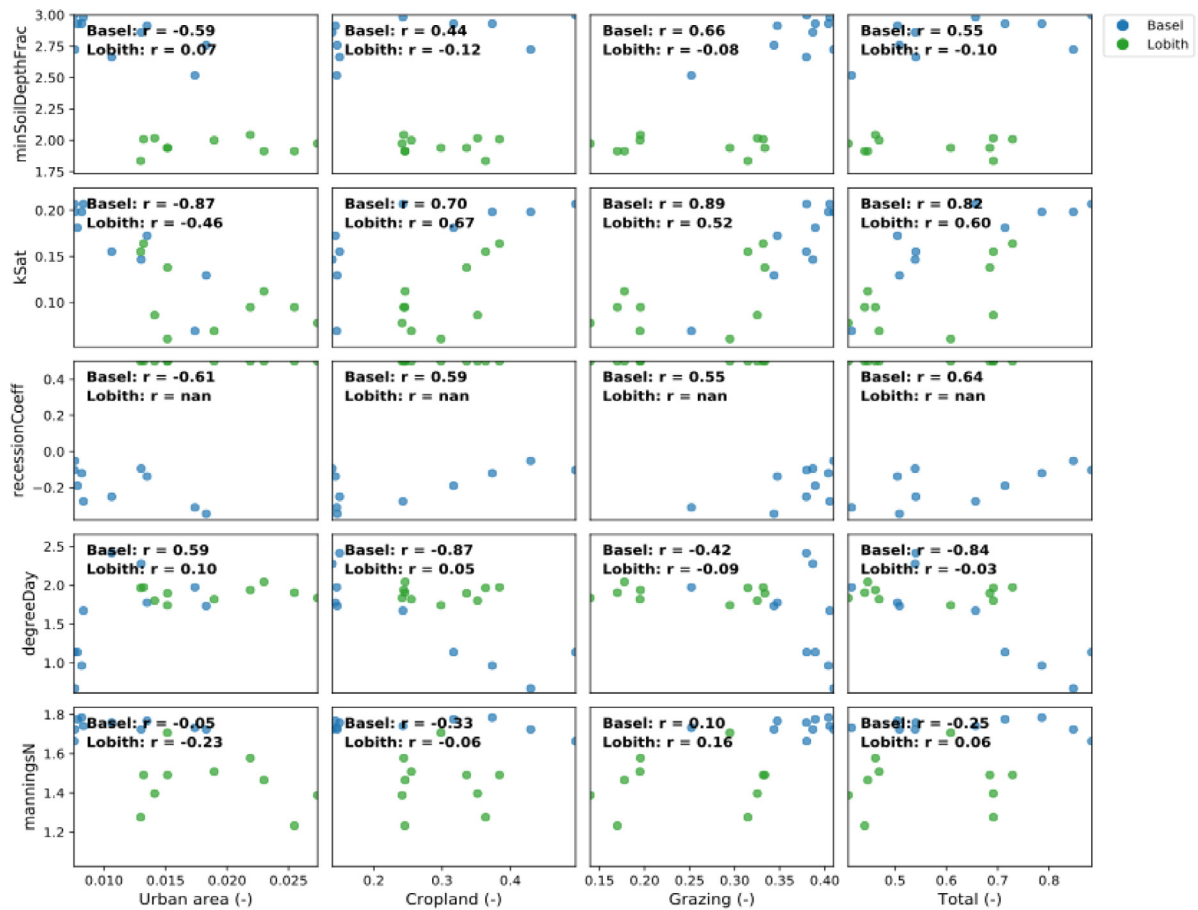


Fig. 10. Scatter plot of parameter multiplication factors and fraction of land use types for Basel (blue) and Lobith (green) and the corresponding correlation coefficient ( $r$ ). Each dot represents one of the years 1910, 1920, 1930, .. 2010. For the scatter plots at the other locations, refer to Digital supplement VIII. (For interpretation of the references to color in this figure legend, the reader is referred to the web version of this article.)

values for saturated hydraulic conductivity and minimum soil depth fraction.

The variations in degree day factor can potentially be explained by a too simplistic snow module in PCR-GLOBWB. Snow melt in PCR-GLOBWB is simulated using temperature index modelling, which is convenient due to its low data requirement and computational simplicity, especially compared to the more physically based energy balance models (Kumar et al., 2013). However, the degree day factor used for the temperature index model often varies considerably in space and time, especially in mountainous areas, due to changes in relative contributions of different heat fluxes (Deng and Zhang, 2018; Jost et al., 2007; Zhang et al., 2006). This could also explain the observed spatial variations in optimal parameter value trends, because the use of temperature index modelling may be sufficient for the downstream areas of the Rhine-Meuse basin (Cochem and Borgharen), but the mountainous areas in the upstream parts may require a more advanced snow melt module to simulate changes in the relative contributions of different heat fluxes (Hock, 2003). For some cases, however, a temperature index model is sufficient (Debele et al., 2010), when the temperature index model is calibrated in space as well as time (Kumar et al., 2013).

Furthermore, because snow melt is modelled on a daily scale, diurnal variations in temperature are not considered. This is important when the temperature is above 0 °C for part of the day, but the average daily temperature is still below freezing. Calibrating the model using both discharge and snow cover data may, therefore, improve the overall model simulations (Franz and Karsten, 2013; Parajka and Blöschl, 2008; Széles et al., 2020), although snow cover data for the first part of the 20<sup>th</sup> century will be difficult to obtain.

#### 4.2.2. Land use change

Contrary to what one might expect, the area of forest has increased in the Rhine-Meuse basin, mainly caused by reforestation as a reaction to the timber shortage after the second world war (Fuchs et al., 2015; Pfister et al., 2004). In the Meuse catchment, this included an increase in coniferous forests (Ashagrie et al., 2006; Tu et al., 2005) and artificially drained agricultural areas (Pfister et al., 2004). Apart from the expansion of irrigated areas, land use change is not included in PCR-GLOBWB (Sutanudjaja et al., 2018). The changes in the land use types (i.e. urban area, cropland, rangeland) are highly correlated (i.e.  $r$  values higher than 0.5 or lower than -0.5) with all parameters except Manning's  $n$ . These high correlations between the changes in land uses and the patterns in optimal parameter values and the fact that land use change is not incorporated in PCR-GLOBWB indicate that land use change is a potential cause of systemic change at the upstream sub-catchments of the Rhine-Meuse basin.

Even though many studies have been carried out to determine the effects of land use change on the discharge or flood frequency (Alewell and Bebi, 2010; Ashagrie et al., 2006; Filoso et al., 2017; Pfister et al., 2004; Pinter et al., 2006; Teuling et al., 2019; Tu et al., 2005; Ward et al., 2008), these effects are complex and it is difficult to provide general conclusions (Tu et al., 2005). The minimum soil depth fraction, hydraulic conductivity and groundwater recession coefficient all show high negative correlations with the amount of urban area and positive correlations with the amount of agricultural area, indicating that both urbanization and a decrease in agricultural area are a possible cause of these parameter changes. Urbanization has been profound in the Rhine-Meuse basin, as the amount of urban area has almost tripled upstream of Basel over

the last century. Streets and houses decrease the infiltration capacity and the removal of vegetation increases transpiration (Hurkmans et al., 2008; Pfister et al., 2004). These processes all increase the runoff coefficient, which, if kept stationary, could be compensated by the decrease in saturated hydraulic conductivity, minimum soil depth fraction and groundwater recession coefficient, as found in this study. Even though only a small fraction (about 2%) of the upstream area of Basel consists of urban area, Hundedcha and Bárdossy (2004) found that urbanization in the middle part of the Rhine catchment has a large effect on the peak flow, especially in summer.

Simultaneously with urbanization, reforestation has occurred in the Rhine-Meuse basin, which expresses itself in the HYDE 3.2 database as a decrease in total 'human' land use. Many studies report that reforestation generally results in a decreased amount of runoff (Alewell and Bebi, 2010; Farley et al., 2005; Filoso et al., 2017; van Dijk and Keenan, 2007), caused by a high evapotranspiration and a high infiltration capacity of forests. Yet, this relation between reforestation and streamflow is expected to depend heavily on the type of forest management (Farley et al., 2005), forest age (Teuling and van Dijke, 2020), and location (Filoso et al., 2017). The positive correlations between the amount of agricultural area and the minimum soil depth fraction; and between the saturated hydraulic conductivity and groundwater recession coefficient suggest an increase in the amount of fast runoff, which contradicts with this general idea that an increase in forest cover results in a decreased runoff. It could therefore be stated that either reforestation is not a cause of systemic change in the Rhine-Meuse basin, or that the link between reforestation and streamflow is indeed not that straightforward.

#### 4.2.3. Construction of river structures

Manning's  $n$  shows, with  $r$  values between -0.35 and 0.51, generally low correlations with patterns in both climate variables and land use types compared to the other parameters. However, some river canalization measures have taken place in the 20<sup>th</sup> century in this study area (Trémoières et al., 1998). The straightening and canalization of the river increases the flow velocity and could therefore explain the decrease in the optimal values of Manning's  $n$  found in, for example, Maxau.

One could argue that the construction of reservoirs and changes in human water use could also affect the discharge and therefore the optimal parameter values over times. However, because these phenomena are both included in PCR-GLOBWB (Sutanudjaja et al., 2018), they should not result in systemic change, unless they are represented too simplistically. In addition, it is expected that reservoirs have a much more abrupt effect on the river discharge than the changes in optimal model parameters observed in our study. It should be noted that the discharge has a relatively low sensitivity to Manning's roughness coefficient compared to other parameters, especially at Basel. This could be an explanation for the small changes in the optimal values of Manning's  $n$  found at Basel and the related low correlations to climate variables and land use types.

#### 4.3. Suggestions for future research

Even though systemic change is a characteristic of a certain catchment in combination with a specific model (Versteegen et al., 2016), it would be interesting to perform the same assessment with a different model. This would show whether the parameter trends found in this study are related to system conceptualizations in PCR-GLOBWB or if there is a more general lack in hydrological process understanding.

In addition, this study only detects systemic change and describes its potential direct causes. Two further lines of research are of interest. Firstly, indirect causes (with and without time lags) should be studied, for example by analysing cross-correlations between potential variables of influence. Secondly, on the basis of our current results, nothing can be said about the consequences of the observed systemic change on future discharge predictions. A next step would, therefore, be to compare

discharge with and without time-variant parameters and validate the predictions with measured discharge values. This way, it can be determined whether systemic change should be considered in future modelling studies or if the differences are neglectable.

## 5. Conclusions

The aim of this study was to identify systemic change in the Rhine-Meuse basin and its potential causes with PCR-GLOBWB 2.0, a global hydrological model. This was done by performing a brute-force calibration for five parameters between 1901-2010. By calibrating for 10-year rolling calibration periods, trends in optimal parameter values through time were determined, indicating the occurrence of systemic change. This led to the following conclusions.

The optimal parameter values, especially the degree day factor, changed notably through time at the upstream calibration locations (Basel and Maxau), with values that ranged from 0.5 to 2.5 times its default value. At the downstream locations (Lobith, Cochem and Borgharen), the optimal parameter values were more stable than at the upstream locations. These changes in optimal parameter values indicate that systemic change has occurred mainly at the upstream subcatchments of the Rhine-Meuse basin, especially in the second half of the 20<sup>th</sup> century.

The high correlations between the optimal parameter values and meteorological forcing and land use data indicate that the both climate change and land use change, mainly urbanization, are potential causes of systemic change in the Rhine-Meuse basin. Canalization of the Rhine could explain the observed changes in Manning's  $n$ .

This study thus shows that systemic change has indeed occurred during the 1901-2010 period in the Rhine-Meuse basin, especially in the more upstream parts. This indicates that future climate change studies that use global or large-scale hydrological models have to be careful when interpreting the results. Especially the optimal value of the degree-day factor shows high variations through space as well as time when PCR-GLOBWB 2.0 is used, which might ask for a more regionalized and time-variant approach.

## Declaration of Competing Interest

The authors declare that they have no known competing financial interests or personal relationships that could have appeared to influence the work reported in this paper

## CRediT authorship contribution statement

**Jessica Ruijsch:** Methodology, Formal analysis, Software, Writing – original draft. **Judith A. Versteegen:** Conceptualization, Writing – review & editing, Supervision. **Edwin H. Sutanudjaja:** Software, Data curation, Writing – review & editing, Supervision. **Derek Karsenberg:** Conceptualization, Writing – review & editing, Supervision.

## Acknowledgment

We would like to thank the anonymous reviewers and the editor for providing constructive comments on the manuscript. We believe that these comments have greatly improved the quality and clarity of this article.

## Supplementary materials

Supplementary material associated with this article can be found, in the online version, at doi:10.1016/j.advwatres.2021.104013.

## References

- Alewell, C., Bebi, P., 2010. Forest development in the European Alps and potential consequences on hydrological regime. In: *Forest Management and the Water Cycle*. Springer, pp. 111–126.

- Arsenault, R., Brissette, F., Martel, J.-L., 2018. The hazards of split-sample validation in hydrological model calibration. *J. Hydrol.* 566, 346–362.
- Ashagrie, A., De Laat, P., De Wit, M., Tu, M., Uhlenbrook, S., 2006. Detecting the influence of land use changes on discharges and floods in the Meuse River Basin—the predictive power of a ninety-year rainfall-runoff relation? *Hydrol. Earth Syst. Sci.* 10 (5), 691–701.
- Bergström, S., 1995. The HBV model. In: *Computer Models of Watershed Hydrology*, pp. 443–476.
- Beven, K., Binley, A., 1992. The future of distributed models: model calibration and uncertainty prediction. *Hydrol. Process.* 6 (3), 279–298.
- Blöschl, G., Bierkens, M.F., Chambel, A., Cudennec, C., Destouni, G., Fiori, A., Kirchner, J.W., McDonnell, J.J., Savenije, H.H., Sivapalan, M., 2019. Twenty-three unsolved problems in hydrology (UPH)—a community perspective. *Hydrol. Sci. J.* 64 (10), 1141–1158.
- Chow, V.T., 1959. *Open-Channel Hydraulics* McGraw-Hill Book Company. New York, pp. 507–510.
- Coron, L., Andréassian, V., Perrin, C., Lerat, J., Vaze, J., Bourqui, M., Hendrickx, F., 2012. Crash testing hydrological models in contrasted climate conditions: An experiment on 216 Australian catchments. *Water Resour. Res.* 48. <https://doi.org/10.1029/2011WR011721>, W05552.
- De Niel, J., Demaréé, G., Willems, P., 2017. Weather typing-based flood frequency analysis verified for exceptional historical events of past 500 years along the Meuse river. *Water Resour. Res.* 53 (10), 8459–8474.
- De Wit, M., Peeters, H., Gastaud, P., Dewil, P., Maeghe, K., Baumgart, J., 2007. Floods in the Meuse basin: event descriptions and an international view on ongoing measures. *Int. J. River Basin Manage.* 5 (4), 279–292.
- Debele, B., Srinivasan, R., Gosain, A., 2010. Comparison of process-based and temperature-index snowmelt modeling in SWAT. *Water Resour. Manage.* 24 (6), 1065–1088.
- Deng, C., Zhang, W., 2018. Spatial distribution pattern of degree-day factors of glaciers on the Qinghai–Tibetan Plateau. *Environ. Monit. Assess.* 190 (8), 1–10.
- Dürr, H.H., Meybeck, M., Dürr, S.H., 2005. Lithologic composition of the Earth's continental surfaces derived from a new digital map emphasizing riverine material transfer. *Glob. Biogeochem. Cycles* 19. <https://doi.org/10.1029/2005GB002515>, GB4S10.
- FAO., 1998. *Digital Soil Map of the World*. Food and Agriculture Organization of the United Nations (FAO).
- Farley, K.A., Jobbágy, E.G., Jackson, R.B., 2005. Effects of afforestation on water yield: a global synthesis with implications for policy. *Glob. Change Biol.* 11 (10), 1565–1576.
- Fernandez-Palominio, C.A., Hattermann, F.F., Krysanova, V., Vega-Jacome, F., Bronstert, A., 2020. Towards a more consistent eco-hydrological modelling through multi-objective calibration: a case study in the Andean Vilcanota River basin, Peru. *Hydrological Sciences Journal* 66 (1), 59–74.
- Filoso, S., Bezerra, M.O., Weiss, K.C., Palmer, M.A., 2017. Impacts of forest restoration on water yield: a systematic review. *PLoS ONE* 12 (8), e0183210.
- Franz, K.J., Karsten, L.R., 2013. Calibration of a distributed snow model using MODIS snow covered area data. *J. Hydrol.* 494, 160–175.
- Fuchs, R., Herold, M., Verburg, P.H., Clevers, J.G., Eberle, J., 2015. Gross changes in reconstructions of historic land cover/use for Europe between 1900 and 2010. *Glob. Change Biol.* 21 (1), 299–313.
- Gupta, H.V., Kling, H., Yilmaz, K.K., Martinez, G.F., 2009. Decomposition of the mean squared error and NSE performance criteria: implications for improving hydrological modelling. *J. Hydrol.* 377 (1–2), 80–91.
- Hagemann, S., Gates, L.D., 2003. Improving a subgrid runoff parameterization scheme for climate models by the use of high resolution data derived from satellite observations. *Clim. Dyn.* 21 (3–4), 349–359.
- Hall, J., Arheimer, B., Borge, M., Brázdil, R., Claps, P., Kiss, A., Kjeldsen, T., Kriaučiūnienė, J., Kundzewicz, Z.W., Lang, M., 2014. Understanding flood regime changes in Europe: a state-of-the-art assessment. *Hydrol. Earth Syst. Sci.* 18 (7), 2735–2772.
- Harris, I., Jones, P.D., Osborn, T.J., Lister, D.H., 2014. Updated high-resolution grids of monthly climatic observations—the CRU TS3. 10 Dataset. *Int. J. Climatol.* 34 (3), 623–642.
- Hock, R., 2003. Temperature index melt modelling in mountain areas. *J. Hydrol.* 282 (1–4), 104–115.
- Hundecha, Y., Bárdossy, A., 2004. Modeling of the effect of land use changes on the runoff generation of a river basin through parameter regionalization of a watershed model. *J. Hydrol.* 292 (1–4), 281–295.
- Hurkmans, R.T.W.L., Terink, W., Uijlenhoet, R., Moors, E.J., Troch, P.A., Verburg, P.H., 2009. Effects of land use changes on streamflow generation in the Rhine basin. *Water Resour. Res.* 45. <https://doi.org/10.1029/2008WR007574>, W06405.
- Hurkmans, R., Terink, W., Uijlenhoet, R., Torfs, P., 2008. Climate change impacts on extreme discharges in the Rhine basin. EMS Annual Meeting & European Conference on Applied Climatology Paper presented at the.
- Ilampooranan, I., Schnoor, J.L., Basu, N.B., 2021. Crops as sensors: using crop yield data to increase the robustness of hydrologic and biogeochemical models. *J. Hydrol.* 592, 125599.
- Isotta, F.A., Frei, C., Weilguni, V., Perčec Tadić, M., Lassegues, P., Rudolf, B., Pavan, V., Cacciamani, C., Antolini, G., Ratto, S.M., 2014. The climate of daily precipitation in the Alps: development and analysis of a high-resolution grid dataset from pan-Alpine rain-gauge data. *Int. J. Climatol.* 34 (5), 1657–1675.
- Jost, G., Weiler, M., Gluns, D.R., Alila, Y., 2007. The influence of forest and topography on snow accumulation and melt at the watershed-scale. *J. Hydrol.* 347 (1–2), 101–115.
- Klein Goldewijk, K., Beusen, A., Van Drecht, G., De Vos, M., 2011. The HYDE 3.1 spatially explicit database of human-induced global land-use change over the past 12,000 years. *Glob. Ecol. Biogeogr.* 20 (1), 73–86.
- Klein Tank, A., Können, G., 2003. Trends in indices of daily temperature and precipitation extremes in Europe, 1946–99. *J. Clim.* 16 (22), 3665–3680.
- Klemeš, V., 1986. Operational testing of hydrological simulation models. *Hydrol. Sci. J.* 31 (1), 13–24.
- Kraijenhoff van de Leur, D., 1958. A study of non-steady groundwater flow with special reference to a reservoir coefficient. *De Ingenieur* 70 (19), B87–B94.
- Kumar, M., Marks, D., Dozier, J., Reba, M., Winstral, A., 2013. Evaluation of distributed hydrologic impacts of temperature-index and energy-based snow models. *Adv. Water Res.* 56, 77–89.
- Lavenne, A.D., Thirel, G., Andréassian, V., Perrin, C., Ramos, M.-H., 2016. Spatial variability of the parameters of a semi-distributed hydrological model. *Proc. Int. Assoc. Hydrol. Sci.* 373, 87–94.
- López López, P., Sutanudjaja, E.H., Schellekens, J., Sterk, G., Bierkens, M.F., 2017. Calibration of a large-scale hydrological model using satellite-based soil moisture and evapotranspiration products. *Hydrol. Earth Syst. Sci.* 21 (6), 3125–3144.
- Melišová, E., Vizina, A., Staponites, L.R., Hanel, M., 2020. The role of hydrological signatures in calibration of conceptual hydrological model. *Water* 12 (12), 3401.
- Merz, R., Parajka, J., Blöschl, G., 2011. Time stability of catchment model parameters: implications for climate impact analyses. *Water Resour. Res.* 47. <https://doi.org/10.1029/2010WR009505>, W02531.
- Murawski, A., Bürger, G., Vorogushyn, S., Merz, B., 2016. Can local climate variability be explained by weather patterns? A multi-station evaluation for the Rhine basin. *Hydrol. Earth Syst. Sci.* 20 (10), 4283–4306.
- Parajka, J., Blöschl, G., 2008. The value of MODIS snow cover data in validating and calibrating conceptual hydrologic models. *J. Hydrol.* 358 (3–4), 240–258.
- Pathiraja, S., Marshall, L., Sharma, A., Moradkhani, H., 2016. Detecting non-stationary hydrologic model parameters in a paired catchment system using data assimilation. *Adv. Water Res.* 94, 103–119.
- Pechlivanidis, I., Jackson, B., McIntyre, N., Wheeler, H., 2011. Catchment scale hydrological modelling: a review of model types, calibration approaches and uncertainty analysis methods in the context of recent developments in technology and applications. *Global NEST J.* 13 (3), 193–214.
- Peel, M.C., Blöschl, G., 2011. Hydrological modelling in a changing world. *Prog. Phys. Geog.* 35 (2), 249–261.
- Pfannerstill, M., Guse, B., Fohrer, N., 2014. Smart low flow signature metrics for an improved overall performance evaluation of hydrological models. *J. Hydrol.* 510, 447–458.
- Pfister, L., Kwadijk, J., Musy, A., Bronstert, A., Hoffmann, L., 2004. Climate change, land use change and runoff prediction in the Rhine–Meuse basins. *River Res. Appl.* 20 (3), 229–241.
- Pinter, N., van der Ploeg, R.R., Schweigert, P., Hoefler, G., 2006. Flood magnification on the River Rhine. *Hydrol. Process.* 20 (1), 147–164.
- Poli, P., Hersbach, H., Dee, D.P., Berrisford, P., Simmons, A.J., Vitart, F., Laloyaux, P., Tan, D.G., Peubey, C., Thépaut, J.-N., 2016. ERA-20C: an atmospheric reanalysis of the twentieth century. *J. Clim.* 29 (11), 4083–4097.
- Scherrer, S.C., Fischer, E.M., Posselt, R., Liniger, M.A., Croci-Maspoli, M., Knutti, R., 2016. Emerging trends in heavy precipitation and hot temperature extremes in Switzerland. *J. Geophys. Res.* 121 (6), 2626–2637.
- Schmidli, J., Frei, C., 2005. Trends of heavy precipitation and wet and dry spells in Switzerland during the 20th century. *Int. J. Climatol.* 25 (6), 753–771.
- Schmitt, L., Morris, D., Kondolf, G.M., 2018. Managing Floods in Large river Basins in Europe: the Rhine river. In: *Managing Flood Risk*. Springer, pp. 75–89.
- Sleziaq, P., Szolgay, J., Hlavčová, K., Duethmann, D., Parajka, J., Danko, M., 2018. Factors controlling alterations in the performance of a runoff model in changing climate conditions. *J. Hydrol. Hydromech.* 66 (4), 381–392.
- Sutanudjaja, E., Beek, L.v., Wanders, N., Wada, Y., Bosmans, J.H., Drost, N., Ent, R.J., De Graaf, I.E., Hoch, J.M., Jong, K.d., 2018. PCR-GLOBWB 2: a 5 arcmin global hydrological and water resources model. *Geosci. Model Dev.* 11 (6), 2429–2453.
- Sutanudjaja, E., Van Beek, L., De Jong, S., Van Geer, F., Bierkens, M., 2014. Calibrating a large-extent high-resolution coupled groundwater-land surface model using soil moisture and discharge data. *Water Resour. Res.* 50 (1), 687–705.
- Sutanudjaja, E., Van Beek, L., De Jong, S.M., Van Geer, F.C., Bierkens, M., 2011. Large-scale groundwater modeling using global datasets: a test case for the Rhine-Meuse basin. *Hydrol. Earth Syst. Sci.* 15 (9), 2913–2935.
- Széles, B., Parajka, J., Hogan, P., Silasari, R., Pavlin, L., Strauss, P., Blöschl, G., 2020. The added value of different data types for calibrating and testing a hydrologic model in a small catchment. *Water Resour. Res.* 56 (10), e2019WR026153.
- Teuling, A.J., De Badts, E.A., Jansen, F.A., Fuchs, R., Buitink, J., Van Dijke, A.J.H., Sterling, S.M., 2019. Climate change, reforestation/afforestation, and urbanization impacts on evapotranspiration and streamflow in Europe. *Hydrol. Earth Syst. Sci.* 23 (9), 3631–3652.
- Teuling, A.J., van Dijke, A.J.H., 2020. Forest age and water yield. *Nature* 578 (7794), E16–E18.
- Thirel, G., Andréassian, V., Perrin, C., 2015. On the Need to Test Hydrological Models Under Changing Conditions. Taylor & Francis Inc.
- Todini, E., 1996. The ARNO rainfall–runoff model. *J. Hydrol.* 175 (1–4), 339–382.
- Trémoлиeres, M., Sánchez-Pérez, J.M., Schnitzler, A., Schmitt, D., 1998. Impact of river management history on the community structure, species composition and nutrient status in the Rhine alluvial hardwood forest. *Plant Ecol.* 135 (1), 59–78.
- Tu, M., Hall, M.J., de Laat, P.J., de Wit, M.J., 2005. Extreme floods in the Meuse river over the past century: aggravated by land-use changes? *Phys. Chem. Earth Parts A/B/C* 30 (4–5), 267–276.
- van Beek, L., & Bierkens, M.M. (2009). *The global hydrological model PCR-GLOBWB: conceptualization, parameterization and verification*. Retrieved from.
- van Beek, L.P.H., Wada, Y., Bierkens, M.F.P., 2011. Global monthly water stress: 1. Water balance and water availability. *Water Resour. Res.* 47. <https://doi.org/10.1029/2010WR009791>, W07517.
- van Dijk, A.I., Keenan, R.J., 2007. *Planted Forests and Water in Perspective*. Elsevier.

- Versteegen, J.A., Karssenbergh, D., van der Hilst, F., Faaij, A.P., 2016. Detecting systemic change in a land use system by Bayesian data assimilation. *Environ. Model. Softw.* 75, 424–438.
- Wada, Y., Wisser, D., Bierkens, M.F., 2014. Global modeling of withdrawal, allocation and consumptive use of surface water and groundwater resources. *Earth Syst. Dyn.* 5 (1), 15–40.
- Wagner, T., McIntyre, N., Lees, M., Wheeler, H., Gupta, H., 2003. Towards reduced uncertainty in conceptual rainfall-runoff modelling: dynamic identifiability analysis. *Hydrol. Process.* 17 (2), 455–476.
- Ward, P.J., Renssen, H., Aerts, J., Van Balen, R., Vandenberghe, J., 2008. Strong increases in flood frequency and discharge of the River Meuse over the late Holocene: impacts of long-term anthropogenic land use change and climate variability. *Hydrol. Earth Syst. Sci.* 12 (1), 159–175.
- Westra, S., Thyer, M., Leonard, M., Kavetski, D., Lambert, M., 2014. A strategy for diagnosing and interpreting hydrological model nonstationarity. *Water Resour. Res.* 50 (6), 5090–5113.
- Winsemius, H.C., Aerts, J.C., Van Beek, L.P., Bierkens, M.F., Bouwman, A., Jongman, B., Kwadijk, J.C., Ligtvoet, W., Lucas, P.L., Van Vuuren, D.P., 2016. Global drivers of future river flood risk. *Nat. Clim. Change* 6 (4), 381–385.
- Yilmaz, K.K., Gupta, H.V., Wagner, T., 2008. A process-based diagnostic approach to model evaluation: application to the NWS distributed hydrologic model. *Water Resour. Res.* 44. <https://doi.org/10.1029/2007WR006716>, W09417.
- Zhang, Y., Liu, S., Ding, Y., 2006. Observed degree-day factors and their spatial variation on glaciers in western China. *Ann. Glaciol.* 43, 301–306.